Process and Mechanism of Phase Separation in Polymer Mixtures with a Thermotropic Liquid Crystalline Copolyester as One Component

Akemi Nakai,[†] Toshio Shiwaku,[‡] Wei Wang, Hirokazu Hasegawa, and Takeji Hashimoto*

Department of Polymer Chemistry, Graduate School of Engineering, Kyoto University, Kyoto 606-01, Japan

Received August 29, 1995; Revised Manuscript Received May 31, 1996[⊗]

ABSTRACT: The phase separation and the coarsening process of polymer mixtures with a thermotropic liquid crystalline polymer (LCP) as one component are investigated. The LCP used is a main-chain type copolyester X-7G, comprised of *p*-hydroxybenzoic acid (60 mol %) and ethylene terephthalate (40 mol %) units. The isotropic, transparent, and homogeneous test specimens of the 50/50 mixtures of X-7G and poly(ethylene terephthalate) (PET) were prepared by a rapid solution-casting with an organic solvent. The specimens were heated rapidly to the test temperature (*T* jump), and an isothermal phase separation process was investigated at real time and *in situ* under a polarized light microscope. A rapid phase separation was observed, when the temperature was higher than the melting points of PET and X-7G, allowing us to study the late stage spinodal decomposition into anisotropic and isotropic liquid phases. The following sequences of the decomposition mechanisms were found as time elapses in this stage: (i) the self-similar growth of a percolating network of the anisotropic liquid phase rich in X-7G in the isotropic matrix phase rich in PET, (ii) disruption of the percolating network and shrinkage of the disrupted fragments into the anisotropic droplets, and (iii) diffusion and coalescence of the anisotropic droplets. The two important factors, transesterification and the liquid crystal effect which can affect the phase separation, are also discussed in the text.

I. Introduction

Structure formation of polymer mixtures via phase separation is an important research theme not only in polymer physics or physical chemistry but also as an interdisciplinary research involving nonequilibrium statistical mechanical studies of complex liquids or soft materials.[1,2] Numerous studies have been reported on the phase separation kinetics, mechanisms, and processes of mixtures composed of amorphous polymers.[3,4] However there have been only a few reports[5−8] on this kind of research for mixtures with a thermotropic liquid crystallline polymer (LCP) as one component. Here, the mixtures, initially in an optically isotropic single phase state, can undergo the phase separation into anisotropic and isotropic liquid phases, giving us an intriguing question on how the coupling between the phase separation and orientational ordering in the LCP-rich phase affects the structure formation. The question should be solved also from the viewpoint of practical application, as briefly given below.

Some commercial main-chain thermotropic LCPs have been mixed with some polymers, forming conventional engineering plastics, in order to improve their mechanical properties. The relationship between the morphology and properties of such kinds of mixtures has been extensively investigated, and the published results have been reviewed in ref 9. Almost all the morphological observations for such polymer mixtures showed a totally separated two-phase structure in a sense that the LCPs are almost immiscible with the flexible chain polymers. Obviously, investigations such as the phase-separation process and control of the supermolecular assembly are very important for practical application in order to prepare high-performance engineering plastics.

This study was also motivated from the following point: the two phases give a remarkable contrast and very clear images by polarized light microscopy (PLM), because one phase is optically anisotropic while the other is optically isotropic. This system may provide an excellent model system with which we can pursue in detail a real space analysis on mechanisms and processes of liquid−liquid phase separation. In our previous work, we have presented preliminary studies of the phase-separation kinetics,[5] processes,[6] and structures[10] in the mixture composed of poly(ethylene terephthalate) (PET), a flexible semicrystalline polymer, and a LCP.

In this paper we present a full description of our experimental results on the isothermal phase-separation processes of the polymer mixtures at a particular temperature range in which the mixture separates into anisotropic and isotropic liquid domains. We will study also the influence of the liquid-crystalline (LC) characteristics of the one component on the phase-separation process.

II. Experimental Methods

The copolyester comprised of *p*-hydroxybenzoic acid (OBA) and ethylene terephthalate (ET) units with a 60/40 mol %/mol % composition (X-7G provided by Tennessee Eastman Co.) and a commercial poly(ethylene terephthalate) (PET) were used as component polymers for a binary mixture. The 50/50 wt %/wt % mixture of X-7G/PET was dissolved into a homogeneous dilute solution with *o*-chlorophenol,[5,6,10] and the transparent, optically isotropic, and homogeneous film specimens with a thickness of ca. 20 μm were prepared by a quick casting method on microscope cover glasses. All the detail methods were given elsewhere.[5,6,10] Hence we describe below only the methods newly employed in this study.

II-A. Determination of Surface Undulation. The film specimens used had a free surface on one side. The phase

[†] Present address: Department of the Home Economics, Kyushu Women's Junior College, 1-1 Jiyugaoka, Yawatanishi, Kitakyushu 807, Japan.

[‡] Present address: Polyplastics Co., Ltd., Research Center, 973 Miyajima, Fuji 416, Japan.

[⊗] Abstract published in *Advance ACS Abstracts,* August 1, 1996.

S0024-9297(95)01276-9 CCC: $12.00

Chart 1

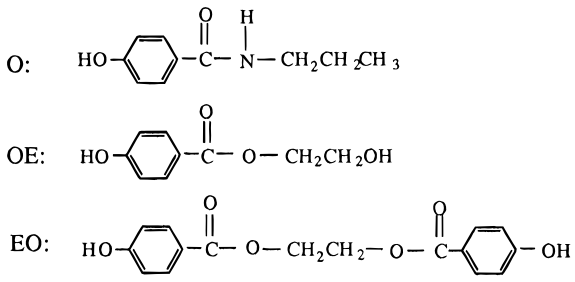

separation may cause a change in the surface topology, and thus the surface undulation or thickness variation of the thin film was determined by a contact profile meter (SE-3FK, Kosaka Institution, Japan). The microscopic origin of the surface undulation was also studied by a Hitachi S-800 scanning electron microscope (SEM) at an accelerating voltage of 10 kV after Pt−Pd sputter coating to prevent charging. For this purpose one of the film specimens was isothermally annealed at 270 °C for 1000 s, quenched to room temperature, and fractured in liquid N_2. The fractured surface and the free surface of this specimen were observed by SEM. The results will be discussed in sections III-D and IV-E.

II-B. Determination of Transesterification between X-7G and PET. The transesterification between X-7G and PET should affect the phase separation kinetics and process, if it occurred. Hence its characterization for the mixture undergoing phase separation is crucial to understand its effects. For this purpose, we applied the chemical degradation method, which was used by Kishiro et al.[11,12] for the analysis of the OBA sequence in the copolyesters of OBA and ET, to our mixtures. In this method, the phase-separated mixture was subjected to the degradation reaction with *n*-propylamine. The relative amount of the three reaction products shown in Chart 1, denoted by [O], [OE], and [EO], respectively, was determined with the ^{1}H-NMR spectra. A parameter [O_E] defined by

$$[O_E] = ([OE] + [EO])/([O] + [OE] + [EO]) \times 100 \quad (1)$$

evaluates the number of the transesterification between X-7G and PET normalized to the total number of OBA segments, the principle of which will be briefly given in Appendix. We determined [O_E] values of the X-7G/PET mixture and neat X-7G as a function of annealing time.

The film specimens of neat X-7G and the X-7G/PET mixture were first annealed at 270 °C for 0−4000 s and then rapidly quenched to room temperature. The vitrified annealed specimens were immersed in *n*-propylamine at room temperature for 24 h and then dried in air. The *n*-propylamine remaining in the solid specimens was removed in a vacuum oven at 50 °C for 2 h. Finally, some soluble fragments formed during the *n*-propylamine treatment in the specimens was extracted by methanol and the chemical structure and the content of the fragments in the solution were determined by ^{1}H-NMR (Bruker NMR AM-500).

II-C. Time-Resolved PLM: Data Acquisition. The phase separation kinetics and the coarsening of the phase-separating domains were investigated by PLM.[5,6,10] The time change in the PLM image was recorded by using a CCD camera and a video recorder. An image taken was converted into a digital data array of 512 × 512 (pixels)^2 at a video rate by using an 8-bit analog-to-digital converter. These digital data could then be analyzed by a personal computer.

The image consists of bright and dark areas (as shown in Figure 1 later) which are anisotropic domains rich in X-7G and isotropic domains rich in PET, respectively. The bright areas contain schlieren textures (as shown in Figure 6 or 7 later), which give a fine brightness distribution in the bright areas. Thus the brightness due to orientation fluctuation of the director in the liquid crystal (LC) phase is coupled with the brightness due to the concentration fluctuations of the LC component and the isotropic component due to phase separation.

II-D. Binarization and Edge Extraction of PLM Images. The PLM image obtained was binarized in order to extract information concerning the spatial concentration fluctuations of the anisotropic and isotropic components (i.e., the concentration order parameter), independently from that associated with the orientation fluctuations in the anisotropic domains (i.e., orientation order parameter). A threshold value for the binarization was chosen, in the range of 135 ± 5 in 8 bit data (0−255) about brightness, so that the original and binarized images are close to each other as much as possible in terms of the concentration order parameter. The binarized image, free from the fine brightness distribution, enabled us to determine the fraction of the anisotropic and isotropic areas, Φ_A and Φ_I (=1 − Φ_A), respectively.

The edges between the bright and dark areas were extracted by numerical execution of the Laplace operators, ∇^2, on the spatial brightness distribution of the images,[13] and the interface length, l_c, between the two coexisting domains was determined from the edge length.

II-E. Determination of Histogram of Characteristic Length. We measured the spatial brightness distribution of the binarized image by scanning it along horizontal and vertical directions. The repeat distance and its histogram thus measured were identical in the two directions and reflect the histogram of a characteristic length, Λ, for the phase-separating structure. We define the probability density $P(\Lambda)$ finding Λ from a frequency of the events $N(\Lambda)$,

$$P(\Lambda) = N(\Lambda)/\int_0^\infty N(\Lambda)\, d\Lambda \quad (2)$$

A normalized probability function $P(\Lambda(t)/\Lambda_m(t))$ is further defined by

$$P(\Lambda(t)/\Lambda_m(t)) \equiv P(\Lambda(t))\Lambda_m(t)/c \quad (3)$$

in order to compare the shape of the distribution function $P(\Lambda(t))$ obtained at different annealing time t. Here Λ_m is the average characteristic length defined by

$$\Lambda_m(t) \equiv \int_0^\infty \Lambda P(\Lambda)\, d\Lambda \quad (4)$$

$P(\Lambda(t)/\Lambda_m(t))$ is dimensionless, and the constant c is defined by

$$\int_0^\infty P(\Lambda(t)/\Lambda_m(t))\, d(\Lambda(t)/\Lambda_m(t)) = 1/c \quad (5)$$

Finally, by plotting $P(\Lambda(t)/\Lambda_m(t))$ against the normalized characteristic length Λ/Λ_m, we can compare the shapes of $P(\Lambda/\Lambda_m)$ obtained at different times. The results will be discussed in sections III-B and IV-A.

III. Experimental Results

III-A. Time Evolution of the Domain Structure. Our previous result[14] showed that at $T_{m,X-7G}$ (≅233 °C) < T < $T_{NN\rightarrow NI}$ (≅370 °C) the phase separation occurs rapidly in the mixture to form the anisotropic domain rich in X-7G and the isotropic domain rich in PET. Here, $T_{NN\rightarrow NI}$ is the transition temperature of the neat X-7G homopolymer from the pure nematic state (defined as NN) to the biphasic region (defined as NI) in which the anisotropic and isotropic liquid phases coexist.[14] $T_{m,X-7G}$ is the melting point of neat X−7G. In this study we chose the test temperatures in the range of 250−280 °C in order to avoid the influence of complicated chemical reactions in the higher temperature range (>300 °C) and vitrification and crystallization of PET and/or X-7G in the lower temperature range (<250 °C).[14]

Figure 1 shows the time evolution of the domain structure as observed by PLM from the same area of the same specimen during the isothermal phase separation after the temperature jump (T jump) to 270 °C. The

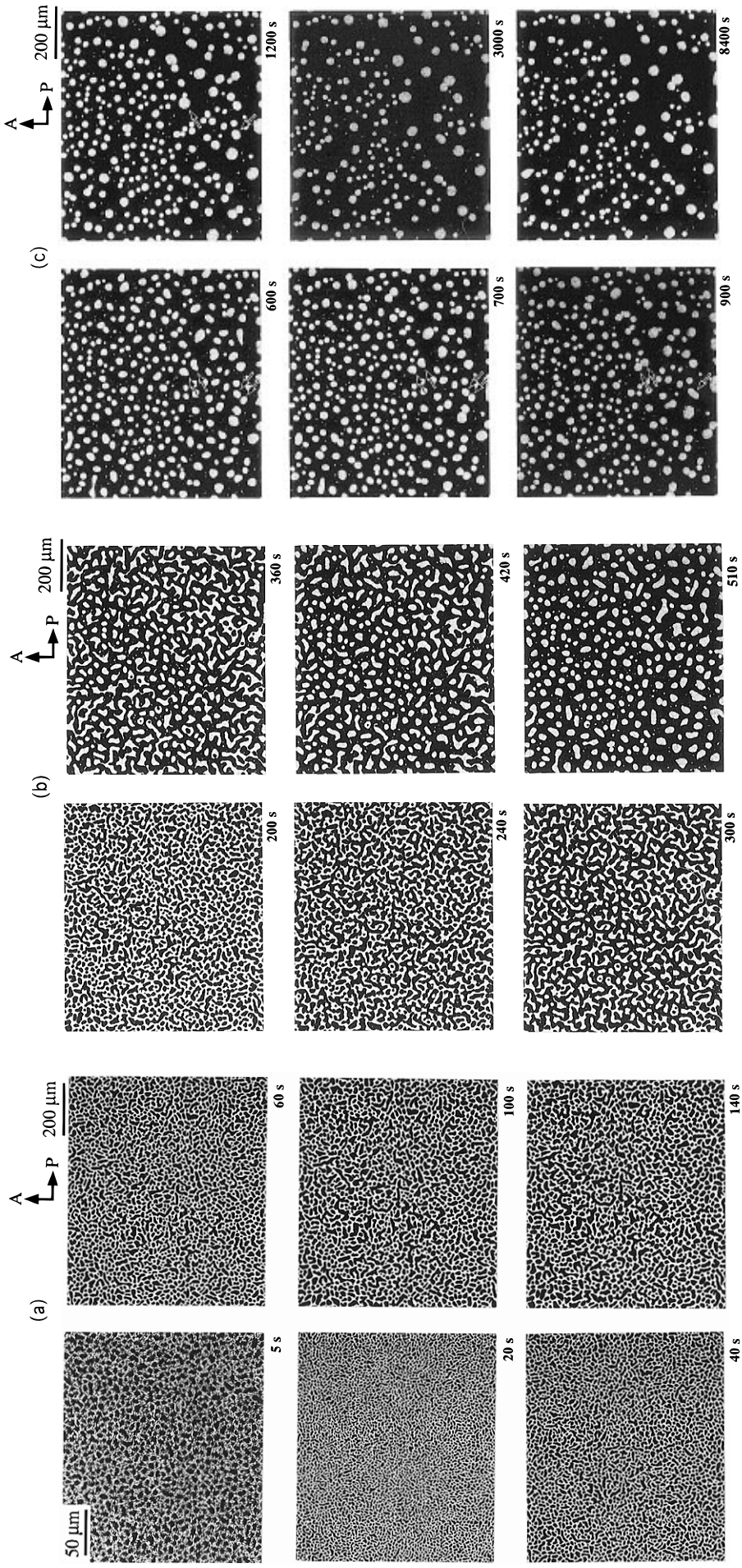

Figure 1. PLM micrographs showing the phase separation process of the X-7G/PET mixture at 270 °C for different annealing times. All the micrographs were obtained from the same area of the same specimen. A and P designate the polarization directions of the analyzer and the polarizer. Bright areas are the anisotropic domains rich in X-7G liquid crystal, and dark areas are the isotropic domains rich in PET melt. Three time regimes are determined according to the characteristics of the domain structure. (a) regime I; (b) regime II; and (c) regime III. Note: only the magnification of the micrograph taken at $t = 5$ s is different from the others.

bright areas on the micrographs are the anisotropic LC domains rich in X-7G, while the dark areas are the isotropic liquid domains rich in PET. All the micrographs were taken with the same magnification, except for the one which was taken at $t = 5$ s with a higher magnification and hence shows a certain fine texture existing in the LC domains (see the top-left micrograph in Figure 1a). For the other micrographs we cannot see any texture inside the LC domains because of a low magnification. The micrograph taken at $t = 5$ s indicates that a bicontinuous network structure, composed of the anisotropic and isotropic domains, is quite rapidly and uniformly formed over the whole sample space. The entire coarsening process can be divided into three regimes, I−III, which are shown in Figure 1a−c, respectively.

In regime I ($5 \lesssim t \lesssim 200$ s), the bright LC phase forms a percolating network in the matrix of the dark isotropic liquid phase and the network grows in size. The fraction of the anisotropic areas, Φ_A, has already reached 0.5 (as quantitatively shown in Figure 14 later) which is nearly equal to the volume fraction of X-7G in the mixture. Φ_A remains constant at 0.5. Furthermore, the domain structure is rapidly transformed from a three-dimensional structure to essentially a two-dimensional structure, because the average characteristic length Λ_m of the domains increases rapidly and then exceeds the thickness of the film specimens at time $t \gtrsim 60$ s (as will be shown in Figure 12, later). Even in the case when the domain structure has the 2D feature at $t \gtrsim 60$ s, the dark phase also forms a continuous phase through thinner parts of the bright network, as will be more clearly shown later in conjunction with Figures 6 and 7. It is intriguing to note that the isotropic liquid phase does not form the percolating network, despite the fact that it also has a volume fraction of 0.5. This may be a consequence of the *LC effect* (see section IV-G later). The mechanism of the phase separation will be discussed in section IV-A.

In regime II ($200 \lesssim t \lesssim 600$ s), the percolating network gradually breaks up into fragments, resulting in the network having only local percolation in the matrix of the isotropic liquid phase. The anisotropic fragments gradually degenerate into the droplets. Thus we find a *percolation-to-cluster (PC) transition* which transforms the percolation structure into a cluster structure composed of the anisotropic droplets dispersed in the isotropic matrix. It is found that in this regime Λ_m increases with t much more rapidly than in regime I and that Φ_A decreases apparently from 0.5 to ca. 0.25, as will be shown more quantitatively in conjunction with Figures 12 and 14 later. The coarsening mechanism will be discussed in section IV-B.

In regime III ($t \gtrsim 600$ s), a phase-separated structure is composed of the anisotropic droplets dispersed in the isotropic matrix. The size of the anisotropic droplets slowly increases with time, as typically demonstrated by the droplets marked by arrows in Figure 1c. Λ_m and Φ_A do not change significantly with t, as will be shown more quantitatively in Figures 12 and 14, respectively, later. The coarsening mechanism in this regime will be discussed in detail in section IV-C.

III-B. Time Changes in Characteristic Length and Its Histogram. The histograms $P(\Lambda)$ of the characteristic lengths $\Lambda(t)$ at various times t after the phase separation are shown in Figure 2 where part a represents those in regimes I and II and part b those in regime III. All curves in the histograms have a single

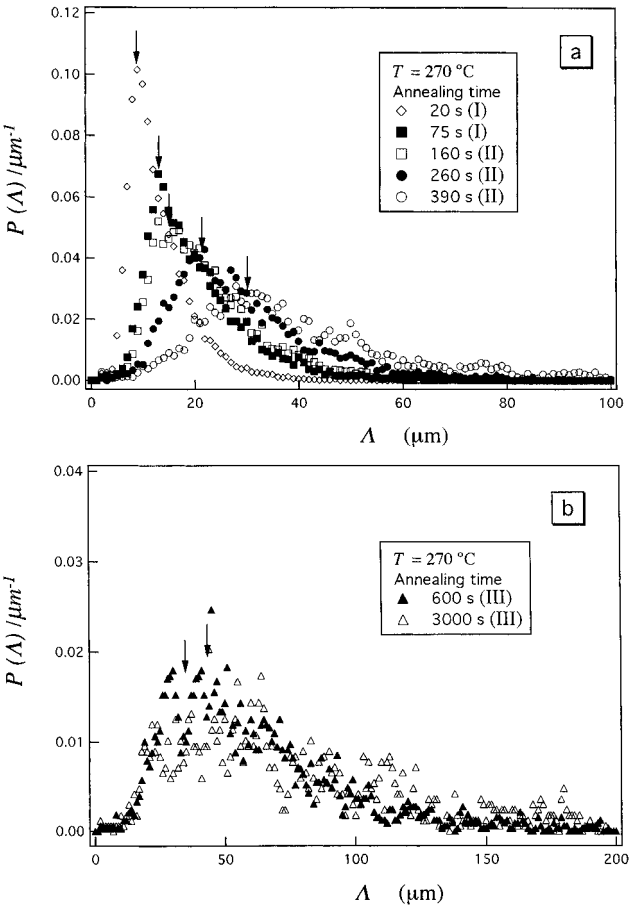

Figure 2. Histograms of the characteristic length Λ determined from the micrographs shown in Figure 1.

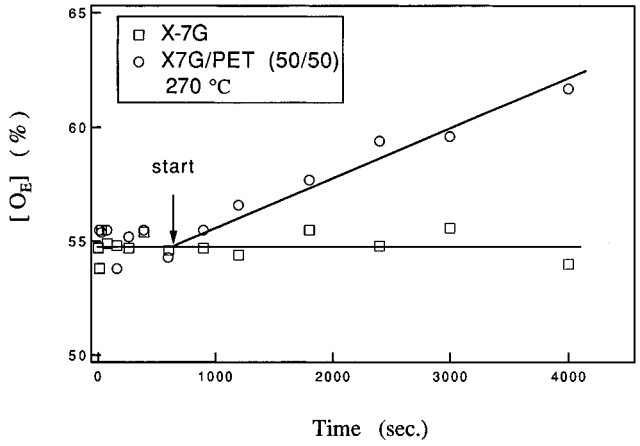

Figure 3. Fraction (%) of ethylene glycol *p*-hydroxybenzoic ester and ethylene glycol di-*p*-hydroxybenzoic ester, $[O_E]$, determined from the neat X-7G and the X-7G/PET mixture as a function of annealing time at 270 °C. The $[O_E]$ for the mixture increases with time from ca. 600 s which corresponds to the beginning of regime III.

peak. The characteristic length at the peak positions $\Lambda_p(t)$ designated by the arrows increases with t. Meanwhile, the peak height decreases with t. It is intriguing to note that the periodicity in the interdroplet distance reflects a memory of a periodic domain structure developed by SD.

III-C. Progress of Transesterification. The quantity $[O_E]$ determined for the pure X-7G and for the mixture are shown as a function of annealing time at 270 °C in Figure 3. For pure X-7G $[O_E]$ is constant at 54.8%, while for the mixture it starts to increase linearly

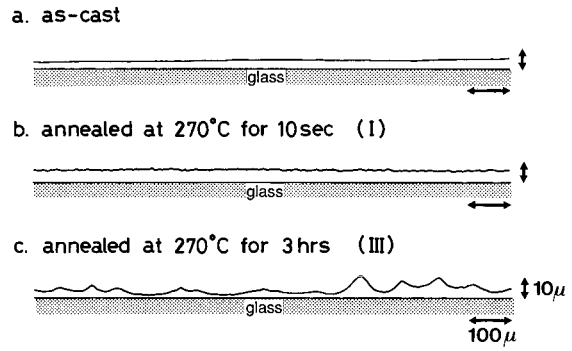

Figure 4. Variation of thickness profiles of the free surface of the X-7G/PET mixture film for (a) as-cast, (b) annealed at 270 °C for 10 s (regime I), and (c) annealed at 270 °C for 3 h (regime III). Due to the shrinkage of the anisotropic domains related to dewetting of the anisotropic liquids from the glass surface, the free surface becomes more uneven in regime III.

with time at $t \gtrsim 600$ s. This means that at 270 °C the detectable transesterification between X-7G and PET starts to occur at $t \gtrsim 600$ s, which corresponds to the beginning of regime III. Thus, effects of the transesterification on the phase separation process should become increasingly important with time in regime III.

III-D. Surface Undulation. In order to understand the origin of the PC transition in regime II, surface roughness was measured as a function of time during the course of the phase separation. Thickness profiles measured for the free surfaces are shown in Figure 4 for three specimens: as-cast film (a), the specimen isothermally annealed at 270 °C for 10 s (regime I) and then quenched to room temperature (b), and the specimen similarly prepared but annealed for 3 h (regime III) (c). These thickness profiles shown here and others taken at different times (not shown here) revealed the time change in the topology of the free surfaces of the film specimens during the phase separation. The results indicate that the surface roughness begins to build up in regime II where the PC transition occurs.

The microscopic origin of the surface roughening was investigated with SEM. Parts a and b of Figure 5 show the SEM micrographs taken with low and high magnifications, respectively, for the X-7G/PET film annealed at 270 °C for 1000 s (in regime III). The micrographs were taken by tilting the specimen by about 30° with respect to the incident beam axis in order to investigate clearly the topology of both the free surface and the fractured surface. To assist the interpretation of the micrograph shown in part b, a corresponding schematic drawing is given in part c. The bright areas in the bottom-right corners of the micrographs in parts a and b correspond to the free surface of the film specimen, while the top-left dark areas correspond to the glass substrate which was fractured together with the film specimen. The structure observed in the center of the micrograph in part b is a hole with the diameter of ca. 20 μm in which an anisotropic droplet existed before the fracturing. As the droplet detached from the matrix and was lost during the fracturing, only a thin shell composed of the isotropic component remained. This micrograph suggests that the isotropic liquid has a lower surface tension than the anisotropic liquid, against both air and the glass surface, and also that the isotropic liquid tends to spread on the glass surface more than the anisotropic liquid. The droplets wrapped up with the isotropic component result in the protrusions on the film surface. The dark (or gray) regions with their shapes elongated parallel to the edge between the glass

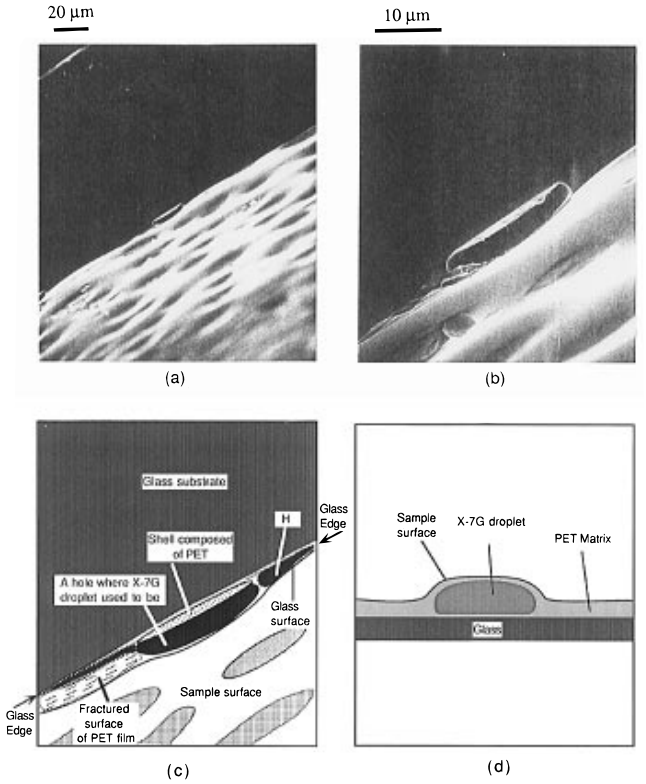

Figure 5. SEM micrographs with low (a) and high magnifications (b) for the mixture annealed at 270 °C for 1000 s, showing the structure of the fractured surface and the free surface. (c) A schematic illustration indicating the characteristics of the SEM micrograph in (b). Hole H resulted from the film being peeled away from the glass during the fracture process. (d) A suggested model which schematically shows a cross section of the two-phase structure of the mixture in regime III.

and the specimen are observed on the free surface in part a (or b). These regions are shown by the shaded regions in part c and correspond to the concave or thinner parts of the film comprised of the phase rich in the isotropic component.

IV. Discussion

IV-A. Ordering Mechanism in Regime I. In Figure 6, four consecutive micrographs taken with high magnification highlight the ordering process of the mixture in regime I. The arrows marked A and B point out two mechanisms, leading to the increase in size of the isotropic domains and the coarsening of the anisotropic network in terms of both Λ_m and their cross sectional area. Arrow A points out a breakup process of a part of the anisotropic network and subsequent relaxation of the local curvature of the interfaces at broken parts. This mechanism was observed more frequently than the other mechanism B. Arrow B points out a small isotropic domain surrounded by the anisotropic phase. The size of this isotropic domain decreased with time and finally disappeared at $t = 148$ s. We note in the time scale covered in Figure 6 that Λ_m is larger than the film thickness, implying that, on average, there is no significant overlap between the anisotropic and isotropic liquids along the thickness direction; i.e., a two-dimensional phase-separated structure is formed. As a possible process occurring in droplet B we can think that the molecules in the small isotropic domain B migrate through the anisotropic domain and then

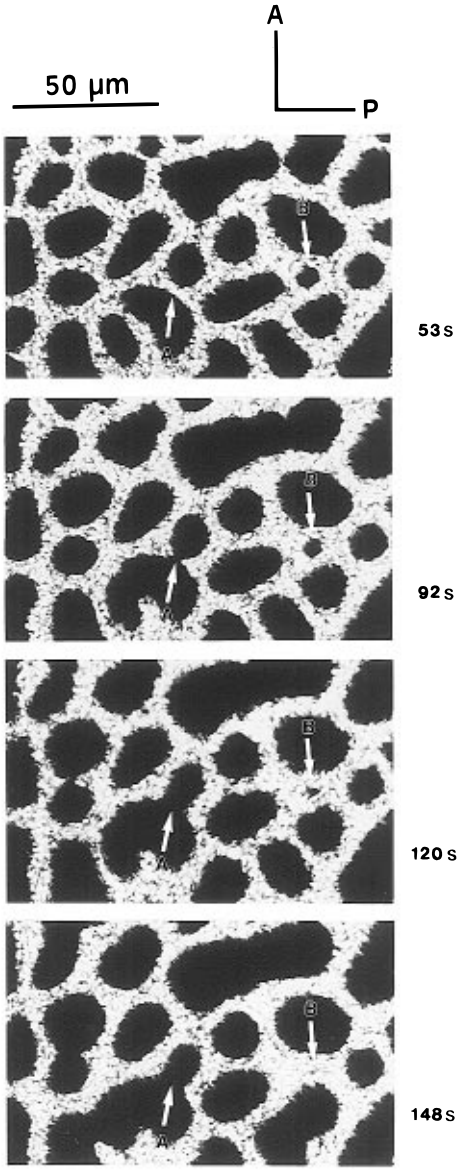

Figure 6. PLM micrographs of the X-7G/PET mixture annealed at 270 °C from 53 to 148 s showing the coarsening processes of the phase-separating domains in the same area. Two mechanisms can be seen in regime I: the breakup and thickening of anisotropic network domains, as pointed out by arrow A, and the diminishing of small isotropic domains surrounded by the anisotropic phase, as pointed out by arrow B.

segregate into neighboring larger isotropic domains, i.e., a typical Lifshitz−Slyozov vaporization−condensation process.[15] However, we cannot rule out another possibility that the isotropic domain B is connected to the surrounding isotropic domains through thin isotropic liquid layers on the top (interfacing with air) or bottom of the anisotropic domain (interfacing with the glass); i.e., the isotropic domains are also continuous, as will be clearly shown from the result in Figure 7 below. If this is the case, the process occurring in droplet B is simply a coarsening process of the anisotropic domains. However, the mechanism involved is still different from that in A.

Figure 7 shows a texture developed in regime I followed by quenching to room temperature. The frozen texture was observed under PLM with two different orientations of polarizer and analyzer. The thin elongated networks marked by arrows appear bright when they are oriented in diagonal directions with respect to

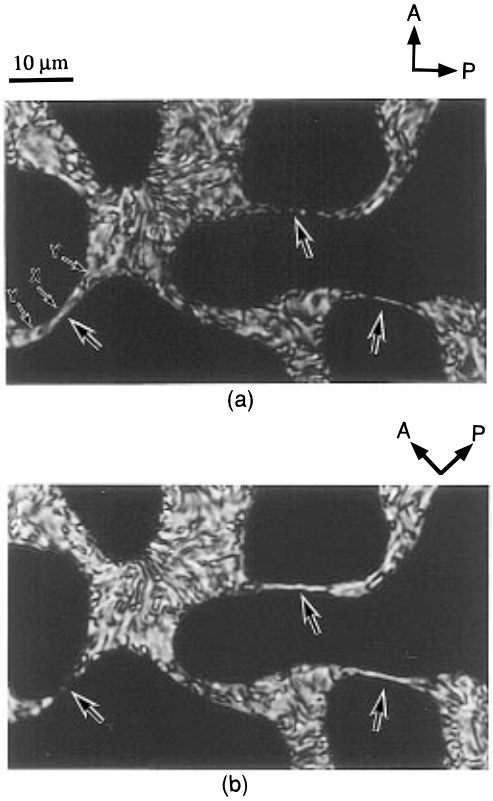

Figure 7. PLM micrographs with two different orientations of the polarizer (P) and the analyzer (A) showing the texture developed at 270 °C for 400 s after the *T* jump followed by quenching to room temperature. Three large arrows point out the thin networks, in which orientation of the liquid crystal molecules are highly coherent, either parallel or perpendicular (more likely parallel) to the network. In micrograph a the parts of the network indicated by arrows Y have thicker diameters and hence have a lower capillary pressure than the part indicated by arrow X. The pressure gradient causes Poiseuille flow and finally the breakup of the network.

the polarizers but dark when they are oriented parallel to one of the polarizers, indicating that the molecules in these anisotropic domains tend to align parallel or perpendicular (more likely parallel) to the network. The thin elongated networks have diameters smaller than the film thickness. Hence the isotropic domains are continuous through the thinner parts of the networks. In this sense, the anisotropic and isotropic domains form a bicontinuous structure. The breakup of the network may be driven by capillary pressure involved in the network:[16] a part of the network Y having a thick diameter has a lower capillary pressure than part X having a thin diameter (see Figure 7a). The pressure gradient may cause Poiseuille flow from the thin part X toward both sides of the thick parts Y. The flow as well as the thermodynamic interaction with the matrix phase may tend to orient liquid crystal molecules either parallel or perpendicular (more likely parallel) to the thin network axis. The schlieren texture seen in the anisotropic domains and a high molecular orientation in the thin parts of the anisotropic domains before the break are the LC effects on the phase-separated structure. The latter may enhance the rate of ordering and be a possible reason why we observe the late stage SD as short as a few 10 s.

Figure 8 shows the three PLM micrographs for the specimen isothermally annealed at 270 °C for 6 (a) and 60 s (b and c) (in regime I). The micrograph shown in part b appears quite different from that in part a at a

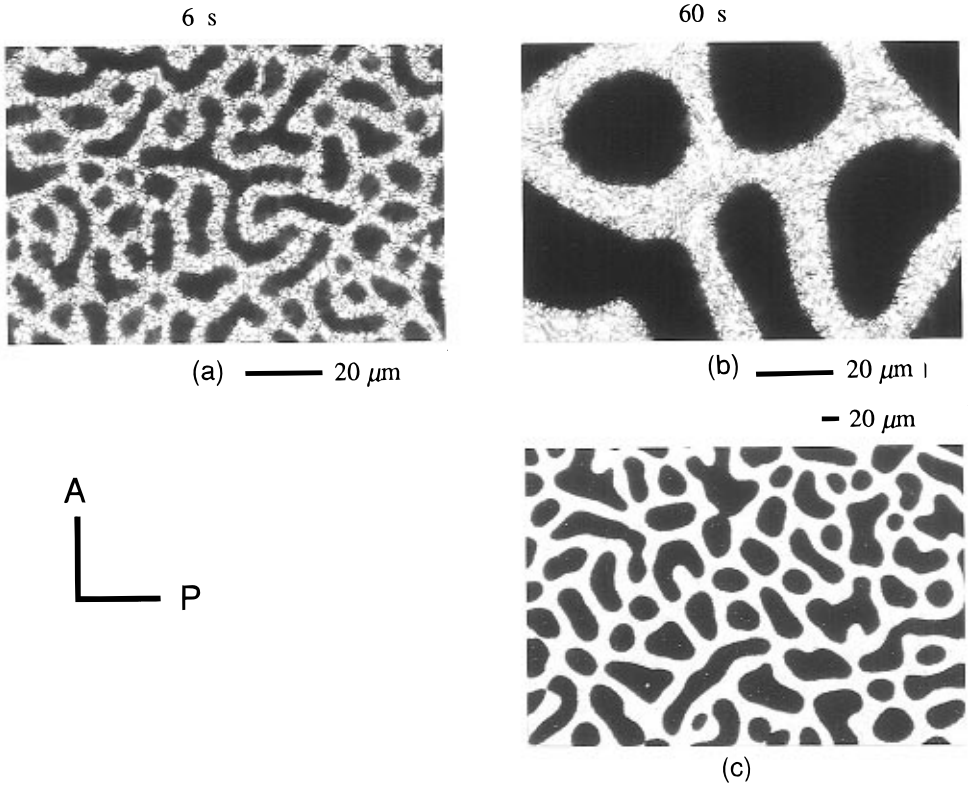

Figure 8. PLM micrographs showing the "self-similar" growth of the domain structure in regime I for the X-7G/PET mixture annealed at 270 °C for 6 and 60 s, respectively. Micrographs a and b were taken at 6 and 60 s with the same magnification. Micrograph c was taken at 60 s but with a lower magnification than (a) and (b).

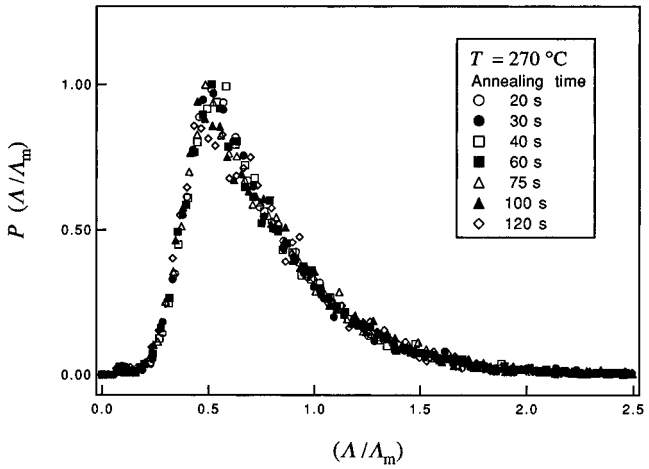

Figure 9. Histogram of the reduced characteristic length Λ/Λ_m, normalized according to eq 5, in regime I for the X-7G/PET mixture annealed at 270 °C. The histogram obtained at the various annealing times, as indicated, falls on a master curve, demonstrating the self-similar growth of the domain structure.

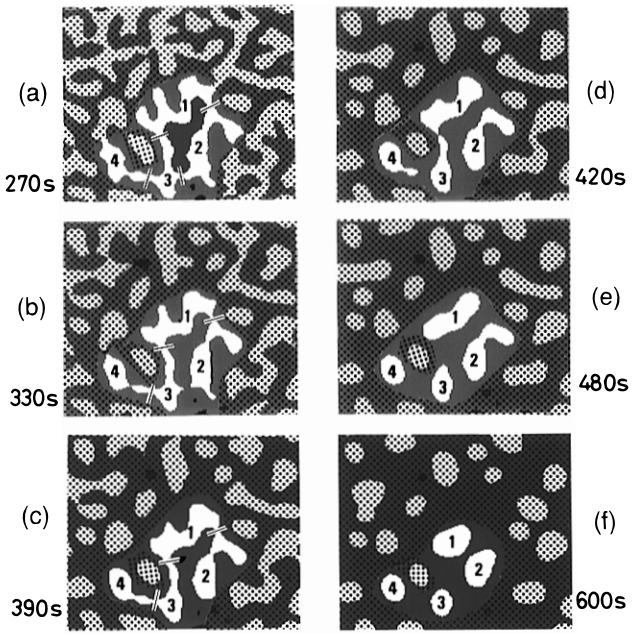

Figure 10. Binarized PLM images obtained on the same area, showing a percolation-to-cluster transition occurring in regime II for the X-7G/PET mixture during isothermal annealing at 270 °C. Shaded or bright domains correspond to the anisotropic networks or droplets rich in X-7G, while dark domains correspond to the isotropic matrix rich in PET. Note that when the bright percolated network in images a−c is divided into four anisotropic fragments numbered 1−4, the centers of mass of these fragments hardly move during the transition process.

glance. However, if the magnification of part b is reduced to ca. one-fifth, as shown in part c, the two images a and c remarkably resemble each other. This result qualitatively implies that the domain structure grows with "dynamical self-similarity" in regime I; i.e., the statistical characteristics of the image (the shape of the domain structure) remain unchanged but only the length Λ_m changes with time.

Figure 9 shows the normalized histograms of $P(\Lambda/\Lambda_m)$ in regime I, obtained by the method discussed in section II-E. The constant c in eq 3 was chosen as the Λ_m value at $t = 20$ s. The seven curves obtained in regime I overlap to form a master curve, giving rise to a reasonable indication that the coarsening process in regime I should be scaled with a time-dependent single length parameter $\Lambda_m(t)$, confirming the dynamical self-similarity. Thus we obtained the following conclusion in regime I: The percolating network structure grows in

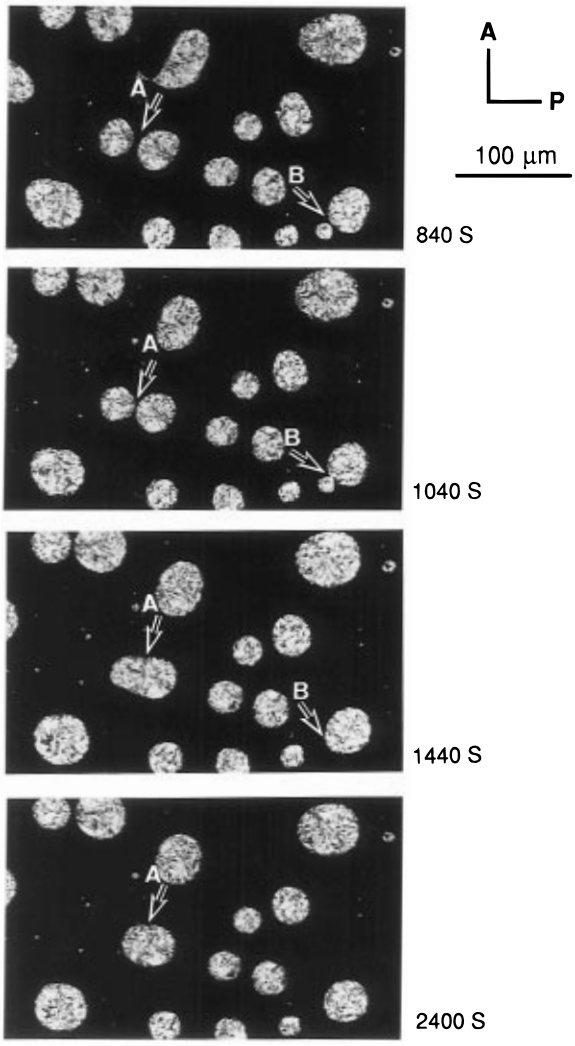

Figure 11. PLM micrographs obtained on the same area, showing the coalescence of anisotropic droplets in regime III for the X-7G/PET mixture at 270 °C. Arrow A points out the coalescence of two large droplets with similar diameters of ca. 25−30 μm, and arrow B, the coalescence of a large and a small droplet with diameters of ca. 35 and 10 μm.

size with dynamical self-similarity through the local breakup of the network, suggesting that this process corresponds to the late stage of spinodal decomposition (SD) of a binary isotropic mixture.[3,4]

IV-B. Ordering Mechanism in Regime II. Figure 10 gives binarized PLM images in regime II at 270 °C. The shaded and bright (unshaded) domains correspond to the anisotropic network or droplets, while the dark domains are the isotropic matrix. Here we focus on the time variation of the bright domains. Part a (t = 270 s) shows the typical bicontinuous domain structure at the end of regime I, while part f (t = 600 s) shows the anisotropic droplet structure at the end of regime II.

The bright percolated network in parts a−c is divided into four fragments, as designated by the numbers 1−4. The boundaries between these fragments at which the network splits into the fragments are indicated by the fine black lines. The splitting process, i.e., the PC transition, is shown by parts a−d. In part d the four isolated fragments are formed. Their centers of mass remain essentially unchanged, but their shapes change from those in part a. The further shrinkage of the fragments is shown from parts d−f, where the droplets of round shapes having the smallest interface area are formed, resulting in lowering the interfacial free energy.

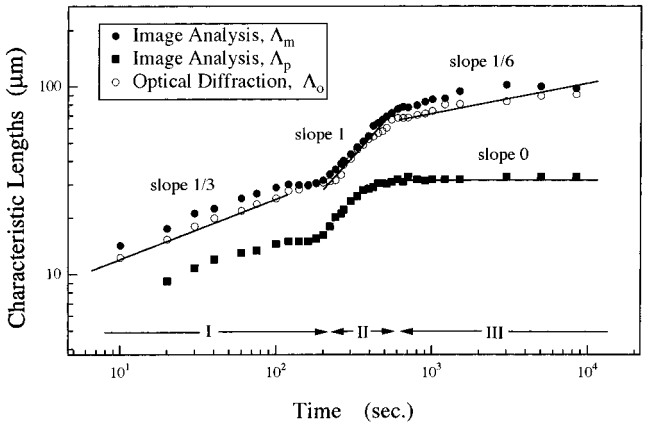

Figure 12. Double logarithmic plots of characteristic lengths Λ_m, Λ_o, and Λ_p *vs* time t for the X-7G/PET mixture at 270 °C. Λ_m was determined according to eq 4, Λ_p from the peak position of the histograms in Figure 2, and Λ_o from the optical diffraction patterns obtained with the binarized PLM images. The three regimes in the coarsening process defined in Figure 1 are indicated in the figure. A linear relation between log Λ and log t can be identified in each regime.

The coarsening process seems to have the following unique features: (i) the internal periodicity within each fragment (spatial concentration fluctuation due to the waviness of the interface) very quickly disappears through rapid relaxation of the local curvature of the interface, but (ii) the external periodicity between the centers of mass of the fragments (concentration fluctuation due to the spatial arrangement of the isotropic and anisotropic domains) hardly or very slowly changes with time. Thus the coarsening in regime II involves the quick relaxation of the internal periodicity, consequently replacing the internal periodicity by the external periodicity.

IV-C. Ordering Mechanism in Regime III. Figure 11 demonstrates the diffusion−coalescence of the anisotropic droplets occurring in regime III, as pointed out by the arrows A and B. Though not obvious in Figure 11, the size of individual droplets might decrease due to the transesterification between X-7G and PET, as described in section III-C.

This coalescence process seems to indicate the mechanism suggested by Nagaya et al.;[8] i.e., large droplets coalesce faster than small droplets. They proposed the diffusion-coalescence of anisotropic droplets driven by an interdroplet attractive interaction which is triggered by the surface tension.[8]

IV-D. Time Evolution of Characteristic Length $\Lambda_m(t)$ in Regimes I, II, and III. Figure 12 shows the time evolution of the characteristic lengths Λ_m (as determined from the binarized images in Figure 1 according to eq 4), Λ_o (as determined from the optical diffraction patterns obtained from the binarized PLM images), and Λ_p (as determined from the peak value in the histogram of $P(\Lambda)$ in Figure 2). It should be noted that the optical diffraction patterns are associated with the concentration order parameter only and show the "spinodal ring". These patterns and their time evolution are consistent with those directly obtained by the light scattering method.[10] Time evolutions $\Lambda_m(t)$, $\Lambda_p(t)$, and $\Lambda_o(t)$ all clearly change in the three regimes defined in Figure 1, verifying again that the ordering mechanisms are different.

In regime I we find

$$\Lambda_m \sim t^{1/3} \tag{6}$$

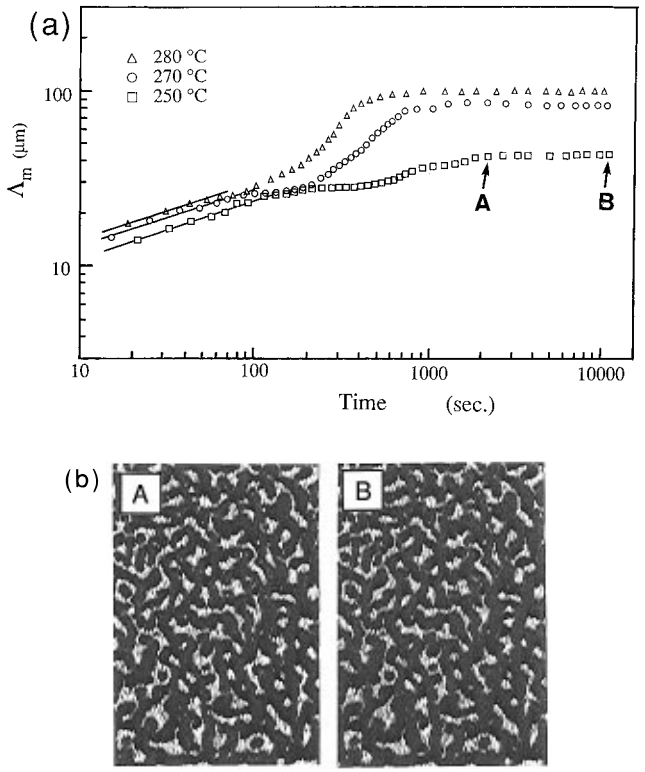

Figure 13. (a) Double logarithmic plots of the average characteristic length Λ_m *vs* time *t* for the X-7G/PET mixture annealed at 250, 270, and 280 °C. (b) PLM micrographs A and B showing the domain structures annealed at 250 °C for 2400 and 10 800 s, respectively, corresponding to the points as indicated by letters A and B in part a.

consistent with our preliminary experimental results.[5,6] Λ_o and Λ_p have time evolutions similar to that of Λ_m. The exponent $^1/_3$ is the one found for the droplet growth caused by the hydrodynamic effect (Brownian coagulation)[17−19] or by the Lifshitz−Slyozov vaporization−condensation process.[15] The exponent is independent of the test temperature, as will be shown in Figure 13a. The primary mechanism found in regime I is the growth of the domains caused by the local instability and breakup of the anisotropic network (see Figure 6).

Siggia[16] and McMaster[20] proposed that the growth and breakup of domains driven by the local instability of networks give the growth law of

$$\Lambda_m \sim t^1 \tag{7}$$

rather than eq 6 for the phase separation of isotropic fluid mixtures. This growth law was also predicted on the basis of interface dynamics for fluid mixtures.[21] McMaster applied Tomotika's instability analysis[22] to predict eq 7. When an infinitely long cylindrical thread of viscous Newtonian fluid with viscosity η' having radius *a* is immersed in another Newtonian fluid with viscosity η, Tomotika's linear analysis predicted that this cylinder becomes unstable, generating undulation in the diameter of the cylinder with wavelength λ and that the transverse disturbance ξ of the cylinder grows exponentially with time *t*where the rate constant α_{max}

$$\xi = \xi_0 \exp(\alpha_{max} t) \tag{8}$$

is given by

$$\alpha_{max} = [\sigma/(2\eta' a)]G(\eta/\eta') \tag{9}$$

σ is the interfacial tension and *G* is a function of only the ratio of the viscosity η/η'. McMaster predicted eq 7 on the basis of the assumption

$$d\Lambda_m/dt \sim (d\xi/dt)_{t=0} = \xi_0 \alpha_{max} = \text{constant} \tag{10}$$

Similarly, Siggia considered that the pressure gradient $\nabla P \sim \sigma/\lambda a$ generated by the undulation in the diameter of the cylinder induces Poiseuille flow along the cylinder axis with the average velocity *v*

$$v \cong 0.1\sigma a/(\eta\lambda) \tag{11}$$

If $a \sim \lambda \sim \Lambda_m$ and $v \cong d\Lambda_m/dt$, then we have

$$d\Lambda_m/dt \cong 0.1(\sigma/\eta) \tag{12}$$

which also predicts eq 7. McMaster assumed that $\xi_0\alpha_{max}$ is independent of time. Siggia assumed that a/Λ_m is a constant independent of time. If a/Λ_m or $\xi_0\alpha_{max}$ is time-dependent and decreases with time

$$\xi_0\alpha_{max} \quad \text{or} \quad a/\Lambda_m \sim t^{-2/3} \tag{13}$$

then $d\Lambda_m/dt$ decreases with time and we can explain our experimental finding of eq 6 instead of eq 7. Whether or not the aspect ratio of the network between the neighboring branching points is conserved during the growth is an intriguing physical problem and deserves future investigation.

In regime II, the relation between Λ_m and *t* follows the power law with the exponent 1 (eq 7). The primary mechanism found for the domain growth in this regime was given in section IV-B. It is interesting to note that the domain growth stops for a while in the time interval between the end of the regime I and the beginning of regime II (ca. 100−250 s). Interpretation of this *intermittent growth* is beyond the scope of the present paper.

In regime III the domain growth law is approximately given by

$$\Lambda_m \sim t^{1/6} \tag{14}$$

In the very late stage of regime III, the droplets become very large and far apart so that the growth of Λ_m with *t* appears to be almost pinned. Figure 12 compares the three characteristic lengths Λ_m, Λ_o, and Λ_p. These values at given times are generally different, because they reflect different moments of $P(\Lambda)$. The values Λ_m and Λ_o are close to each other but much larger than Λ_p. This difference is associated with asymmetry and breadth in $P(\Lambda)$. The time dependence of Λ_p is different from that of Λ_m, slight in regimes I and II but large in regime III.

Figure 13a shows the influence of the annealing temperature on the time evolution of the characteristic length Λ_m. It is worthwhile to note that in regime I the time evolution of Λ_m at the three temperatures obeys the same power law, indicating that the mechanisms of the phase separation in this regime are identical; only the time scales are different: the higher the temperature, the faster the growth of Λ_m, due to larger mobility. The time evolution of Λ_m at 250 °C is pinned in the later stage which is caused by crystallization of the PET component.[10] Owing to the pinning effect, regimes II and III do not appear at 250 °C: the PC transition did not occur. This is clearly indicated by the two almost same PLM images in Figure 13b, taken at 2400 (des-

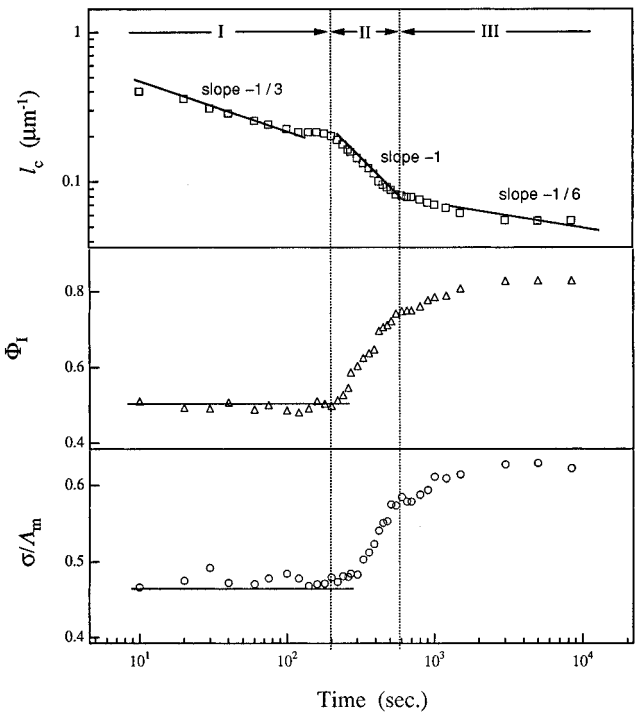

Figure 14. Time changes in the interfacial length per unit area l_c, the area fraction of the isotropic domain Φ_I, and the ratio of FWHM of the histograms $P(\Lambda)$ to the average characteristic length σ/Λ_m for the X-7G/PET mixture annealed at 270 °C.

ignated as A) and 10 800 s (designated as B). Thus the coarsening process was pinned in the beginning of regime II. The crossover from regime II to III occurs earlier at 280 °C than at 270 °C: the PC transition in regime II occurs faster at 280 °C. Thus the crossover seems to occur at a given length scale inherent in the system.

In order to further help understanding of the nature of the phase separation and the coarsening mechanism, three parameters, the interface length l_c per unit area, the area fraction of isotropic component Φ_I, and the ratio σ/Λ_m, are plotted as a function of the annealing time in Figure 14. Here σ is the full width at half-maximum (FWHM) of $P(\Lambda)$. It is clearly seen that the interface length (hence the interface area per unit volume) decreases with time. Time dependencies of l_c^{-1} and Λ_m are extremely alike and given by

$$l_c^{-1} \sim \Lambda_m \sim t^{\alpha} \qquad (15)$$

with $\alpha = {}^1/_3$, 1, ${}^1/_6$, and 0 for regime I, regime II, the early phase of regime III, and the late phase of regime III, respectively. The fact that the phase-separated structure is scaled with the single length parameter l_c^{-1} or Λ_m reveals an important piece of evidence in the ordering process: the relaxation rate of the interface undulation is faster than or equal to Λ_m so that l_c^{-1} cannot be a parameter independent of Λ_m. This finding is consistent with our earlier experimental findings for isotropic liquid mixtures of polymers.[23,24] If the relaxation rate of the interface undulation is slower than the growth rate of Λ_m, the exponent α for l_c^{-1} should be smaller than that for Λ_m, and the interface becomes very wavy.

The nature of phase separation and the coarsening mechanism can also be explored in terms of the time dependence of σ/Λ_m. In regime I, σ/Λ_m is constant, as is obvious from the master curve obtained for $P(\Lambda/\Lambda_m)$ in Figure 9, indicating that the ordering process is scaled with the single length parameter Λ_m in this regard as well. In regime II, σ/Λ_m rapidly increases due to the PC transition, as shown in Figure 10. In the late phase of regime III, σ/Λ_m is independent of time again. However, in the early phase of regime III, σ/Λ_m slightly increases.

IV-E. Surface Roughening Transition. The results shown in section III-D show that the surface roughness gradually appears in regime II, but it becomes significant in the time interval between the end of regime II and the beginning of regime III. Moreover, this surface roughening transition was associated with the protrusion of the anisotropic droplets from the isotropic matrix phase.

We found that the surface roughening transition, the PC transition, and the apparent decrease of the area fraction of the anisotropic phase Φ_A occur in parallel in regime II. At this stage we cannot clarify basic physical factors underlying these phenomena and interrelations among these phenomena. As a key physical factor, however, we may point out a difference of wettability of the two phases against the glass surface and air. Based on the study by SEM shown in Figure 5, we know that the surface roughness of the films in regime III (Figure 4) were caused by the protrusion of the anisotropic droplets.

IV-F. Effect of Transesterification. It is well-known that the transesterification between two components can change the structure and properties of the multicomponent systems consisting of two or more polyesters.[25,26] It is also important to emphasize that the copolyesters of OBA and ethylene terephthalate cannot form a liquid crystal phase when the content of OBA is less than 30 mol %.[27] The transesterification between X-7G sequences and pure PET sequences might result in the copolyester having the content of OBA less than 30 mol %, and hence the fraction of the isotropic phase Φ_I may increase during the isothermal annealing process. For the X-7G/PET mixture, however, the observed increase in Φ_I in regime II (Figure 14) is not due to the transesterification between the two components in the mixture in light of the results obtained in Figure 3; i.e., the transesterification is detectable only after entering into regime III. For the mixture studied, the unmixing into two phases was achieved in 5 s at 270 °C, as shown in Figure 1. Therefore, the transesterification between the two components can significantly *occur only in the interfacial areas*. This means that this reaction in our system is very limited as compared with that occurring in the miscible mixtures.[25,26] It is clear now that the observed increase in Φ_I in regime II is not due to the transesterification.

IV-G. Summary of Effects of the LC Phase on the Phase Separation. We studied the process and mechanism of the liquid−liquid phase separation of the 50/50 wt %/wt % mixture of X-7G/PET at the given temperatures. The phase separation process and mechanism of this system are found to be generally very similar to those of isotropic liquid mixtures. For example, the scaling relation (eq 6) in regime I is the same as that of ordinary binary polymer mixture systems. Nevertheless, we try to point out below the LC effects on the phase separation of this mixture.

We observed only the late stage SD[3,4] at the given temperatures even in the time range of a few 10 s. This fact may indicate that the LC characteristic of one

component (X-7G) results in a rapid phase separation. This LC effect arises from a large segregation power of the LCP against the flexible PET[28] and a low viscosity of the nematic LCP phase. The latter is primarily due to the alignment of the directors induced by flow in the LCP network which, in turn, is driven by the capillary pressure. The LC effect will increase the prefactor of the scaling relation (eq 6). The intriguing observation that the LC phase, instead of the isotropic liquid phase, forms the percolating network in regime I may be attributed to a dynamical asymmetry;[29] i.e., the viscosity of the LC phase is smaller than that of the isotropic phase.

The liquid crystal domains show the schlieren texture typical of the nematic phase, as shown in Figures 7 and 11. However, how the texture of the LCP formed in the phase-separating domains is different from that formed in the neat LCP is left unsolved. The nematic ordering in the LCP domains may be well expected to be affected by the interface with the flexible polymers. The surface roughening transition accompanied by the PC transition may also be the effect unique to the system having the LCP domains.

V. Summary

The phase separation and the ordering process of the X-7G/PET mixture were investigated at the test temperatures higher than the melting points of X-7G and PET but lower than nematic-to-biphasic transition of the neat X-7G. The results obviously indicated the phase separation into the anisotropic and isotropic liquid phases according to SD. Only the late stage SD was observed even at the shortest time scale of our observation (a few 10 s), which may be due to a high segregation power between the LCP and the PET and a large mobility of the LCP domains. The ordering process in the late stage was found to consist of regimes I−III in the time sequence. In regime I a percolating network of the anisotropic phase rich in X-7G (not of the isotropic phase rich in PET), grows with a dynamical self-similarity in the isotropic matrix rich in PET. The characteristic length Λ_m of the domains is scaled as $\Lambda_m \sim t^{1/3}$, similarly to ordinary binary polymer mixture systems. In regime II the percolating network breaks up into the fragments and the fragments degenerate to form optically anisotropic droplets in the isotropic matrix, showing a percolation-to-cluster transition and apparently increasing the area fraction of the isotropic phase. This process was interrelated to give the surface roughening transition driven by the wettability difference of the two phases against the glass surface and air. In this regime, Λ_m is scaled as $\Lambda_m \sim t^1$. In regime III the coarsening process is controlled by the diffusion and coalescence of the anisotropic droplets and Λ_m slowly increases with time, giving rise to the scaling relation $\Lambda_m \sim t^{1/6}$ or $\Lambda_m \sim t^0$. An intriguing intermittency in the growth of $\Lambda_m(t)$ was observed in the time scale between regimes I and II.

Acknowledgment. We are grateful to Dr. O. Kishiro and Mr. Y. Sakata, Mitsubishi Chemical Co. Ltd., Japan, for kindly suggesting the analysis of the transesterification between X-7G and PET. This work is supported in part by a Grant-in-Aid for Scientific Research on Priority Areas, "Cooperative Phenomena in Complex Liquids", Ministry of Education, Science, Sports, and Culture, Japan.

Scheme A

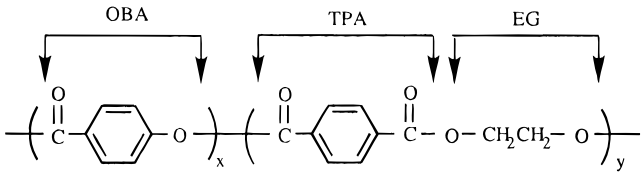

Appendix. Determination of Transesterification

Here, we describe briefly only the principle of the method, to help understand this technique, but leave the details to Kishiro et al.[11,12]

X-7G consists of three kinds of segmental units, as shown in Scheme A: OBA (the units based on *p*-hydroxybenzoic acid), TPA (terephthalic acid), and EG (ethylene glycol). Four kinds of linkages are formed between these segmental units, i.e., OBA−OBA, OBA−TPA, OBA−EG, and TPA−EG. OBA−OBA and OBA−TPA linkages are attacked by *n*-propylamine, and then scission of the linkages occurs quite fast, whereas scission of TPA−EG linkages proceeds rather slowly. In contrast, OBA−EG linkages are stable for the *n*-propylamine treatment. If we focus on the OBA units, the possible sequences related to OBA in X-7G are classified into the following seven cases:

(a) −OBA−OBA−OBA−

(b) −TPA−OBA−OBA−

(c) −OBA−OBA−EG−TPA−

(d) −TPA−OBA−EG−TPA−

(e) −OBA−OBA−EG−OBA−OBA−

(f) −TPA−OBA−EG−OBA−OBA−

(g) −TPA−OBA−EG−OBA−TPA−.

Among them, sequences b−g can result from transesterification between the OBA sequence (sequence a) and PET sequence (−TPA−EG−TPA−EG−). Only three kinds of fragments as listed in Chart 1 in section II-B are produced from the degradation of these seven OBA-containing sequences. Sequences a and b degrade and produce fragment O (*N*-propyl-4-hydroxybenzamide). Similarly, fragment OE (ethylene glycol *p*-hydroxybenzoic ester) is produced from sequences c and d, and fragment EO (ethylene glycol di-*p*-hydroxybenzoic ester) from sequences e−g. The relative contents of fragments of O, OE, and EO, denoted by [O], [OE], and [EO], respectively, can be obtained from the ^{1}H-NMR spectra. The sum of [O], [OE], and [EO] is proportional to the content of OBA segments in X-7G, because the transesterification does not change the content of OBA segment but just alters the sequence distribution of OBA, TPA, and EG. The transesterification between PET and X-7G increases the content of TPA and EG segments in X-7G and that of OBA segments in PET, which causes an increase in sequences c−g, and hence an increase in [OE] and [EO], or a decrease in [O]. (An increase in sequence b resulting from the transesterification does not change [O] but the counterpart sequence produced at the same time, −OBA−EG−, increases [OE] or [EO].) On the other hand, the transesterification within X-7G does not change the content of TPA and EG segments and hence the total number

of sequences c−g, which causes no change in [OE] and [EO]. Thus $[O_E]$ in eq 1 evaluates the number of the transesterification between X-7G and PET normalized to the total number of OBA segments.

References and Notes

(1) *Dynamics of Ordering Processes in Condensed Matter*; Komura, S., Furukawa, H., Eds.; Plenum: New York, 1988.
(2) *Dynamics and Patterns in Complex Fluids*; Onuki, A., Kawasaki, K., Eds.; Springer: Berlin, 1990.
(3) Hashimoto, T. *Phase Transition* **1988**, *12*, 47.
(4) Hashimoto, T. In *Materials Science and Technology*; Cahn, R. W., Haasen, P., Kramer, E. J., Eds. Structure and Properties of Polymers, Vol. 12; Thomas, E. L., Vol. Ed.; VCH: Weinheim, 1993; Chapter 6.
(5) Nakai, A.; Shiwaku, T.; Hasegawa, H.; Hashimoto, T. *Macromolecules* **1986**, *19*, 3008.
(6) Hasegawa, H.; Shiwaku, T.; Nakai, A.; Hashimoto, T. In *Dynamics of Ordering Processes in Condensed Matter*; Komura, S., Furukawa, H., Eds.; Plenum: New York, 1988; p 457.
(7) Kyu, T.; Zhang, P. *Polym. Commun.* **1988**, *29*, 99.
(8) Nagaya, T.; Orihara, H.; Ishibashi, Y. *J. Phys. Soc. Jpn.* **1989**, *58*, 3600.
(9) Dutta, D.; Fruiwala, H.; Kohli, A.; Weiss, R. A. *Polym. Eng. Sci.* **1990**, *30*, 1005 and the literature therein.
(10) Nakai, A.; Shiwaku, T.; Wang, W.; Hasegawa, H.; Hashimoto, T. *Polymer* **1996**, *37*, 2259.
(11) Sakata, Y.; Kishiro, O. *Polym. Prepr., Jpn.* **1993**, *42*, 1233.
(12) Sakata, Y.; Kishiro, O. Manuscript in preparation.
(13) *Digital Picture Processing*; Rosenfeld, A., Kak, A. C., Eds.; Academic: New York, 1976.
(14) Shiwaku, T.; Nakai, A.; Hasegawa, H.; Hashimoto, T. *Macromolecules* **1990**, *23*, 1590.
(15) Lifshitz, I. M.; Slyozov, V. V. *Phys. Chem. Solids* **1961**, *19*, 35.
(16) Siggia, E. D. *Phys. Rev. A* **1979**, *20*, 595.
(17) Binder, K.; Stauffer, D. *Phys. Rev. Lett.* **1974**, *33*, 1006.
(18) Furukawa, H. *Prog. Theor. Phys.* **1978**, *59*, 1072; *Phys. Rev. Lett.* **1979**, *43*, 136; *Phys. Rev. A* **1981**, *23*, 1535; *Physica A (Amsterdam)* **1984**, *123*, 479.
(19) Kawasaki, K.; Ohta, T. *Prog. Theor. Phys.* **1978**, *59*, 362.
(20) McMaster, K. T. *Adv. Chem. Ser.* **1975**, *142*, 43.
(21) Kawasaki, K. *Ann. Phys. N.Y.* **1984**, *154*, 319.
(22) Tomotika, S. *Proc. R. Soc. London, Ser. A* **1935**, *150*, 322; **1936**, *153*, 302.
(23) Hashimoto, T.; Takenaka, M.; Jinnai, H. *J. Appl. Crystallogr.* **1991**, *24*, 457.
(24) Takenaka, M.; Hashimoto, T. *J. Chem. Phys.* **1992**, *96*, 6177.
(25) MacDonald, W. A.; McLenaghan, A. D. W.; McLean, G.; Richards, R. W.; King, S. M. *Macromolecules* **1991**, *24*, 6164.
(26) Kugler, J.; Gilmer, J. W.; Wiswe, D.; Zachmann, H.-G.; Hahn, K.; Fisher, E. W. *Macromolecules* **1987**, *20*, 1116.
(27) Jackson, W. J.; Kuhfuss, H. F. *J. Polym. Sci., Polym. Chem. Ed.* **1976**, *14*, 2043.
(28) Lui, A. J.; Fredrickson, G. H. *Macromolecules* **1992**, *25*, 5551; **1993**, *26*, 2817.
(29) Onuki, A. *Europhys. Lett.* **1994**, *28*, 175.

MA9512768